

## Research Article

# Solid Solubility in $\text{Cu}_5\text{Gd}_{1-x}\text{Ca}_x$ System: Structure, Stability, and Hydrogenation

Andraž Kocjan,<sup>1</sup> Luka Kelhar,<sup>1,2</sup> Anton Gradišek,<sup>1</sup> Blaž Likozar,<sup>3</sup> Kristina Žagar,<sup>1,2</sup> Jaafar Ghanbaja,<sup>2,4</sup> Spomenka Kobe,<sup>1,2</sup> and Jean-Marie Dubois<sup>2,4</sup>

<sup>1</sup>Jožef Stefan Institute, Jamova cesta 39, SI-1000 Ljubljana, Slovenia

<sup>2</sup>International Associated Laboratory and PACS2 and CNRS Nancy and JSI, Ljubljana, Slovenia

<sup>3</sup>Department of Catalysis and Chemical Reaction Engineering, National Institute of Chemistry, Hajdrihova 19, SI-1001 Ljubljana, Slovenia

<sup>4</sup>Institut Jean Lamour (UMR 7198 CNRS-Université de Lorraine), Parc de Saurupt, CS50840, 54011 Nancy Cedex, France

Correspondence should be addressed to Anton Gradišek; [anton.gradisek@ijs.si](mailto:anton.gradisek@ijs.si)

Received 16 November 2016; Accepted 29 January 2017; Published 13 March 2017

Academic Editor: Pavel Lejcek

Copyright © 2017 Andraž Kocjan et al. This is an open access article distributed under the Creative Commons Attribution License, which permits unrestricted use, distribution, and reproduction in any medium, provided the original work is properly cited.

We report on synthesis and characterization of a novel group of compounds based on copper, gadolinium, and calcium. Cu-Ca and Cu-Gd binaries were previously studied while Ca and Gd are known to be immiscible themselves. The effects of substituting Gd with Ca in  $\text{Cu}_5\text{Gd}_{1-x}\text{Ca}_x$  compounds ( $0 \leq x \leq 1$ ) were studied by investigating the phase stability and crystal structure of the resulting new compounds in five specimens with  $x = 0, 0.33, 0.50, 0.66,$  and  $1$ , respectively. The samples produced by melt-spinning had hexagonal P6/mmm structure, irrespective of Ca amount ( $x$ ), where lattice parameters varied with  $x$  linearly. This is an indication of good solid solubility under the preparation conditions. A slower cooling upon arc-melting caused the liquid phase separation into  $\text{Cu}_{4.5}\text{Gd}$  and Cu-Ca compounds. Using TEM, rapidly solidified ribbons ( $\text{Cu}_5\text{Gd}_{0.5}\text{Ca}_{0.5}$ ) were investigated and the formation of a homogeneous ternary phase with a nearly nominal stoichiometric composition and minor amounts of Cu-Ca secondary phase was observed. Using DSC and HT XRD, we found that these systems are stable at least up to  $400^\circ\text{C}$ . Upon a 16-hour hydrogenation at 1 bar and  $300^\circ\text{C}$ , all specimens absorbed about 0.5 wt.% of hydrogen. This caused changes in structure with the formation of pure Cu and  $\text{H}_2\text{Gd}_{1-x}\text{Ca}_x$  solid solution.

## 1. Introduction

A number of empirical rules based on thermodynamic criteria have been developed to predict the formation of solid solutions in metallic systems. Hume-Rothery rules [1] were used for decades in traditional alloy design, as they postulate the conditions for substitutional solid solubility in binary systems, that is, the same crystal structure and valence state, similar electronegativity, and a difference in atom sizes between solute and solvent atoms that should be less than 15%. However, for alloys with more than two constituent elements, especially for the so-called high entropy alloys (HEA), which contain five or more elements in equimolar ratio, other rules and parameters must be applied, as reported by Takeuchi and Inoue [2], Zhang et al. [3], and Guo et al. [4, 5]. These authors derived several empirical criteria which can

be applied for phase selection and stability in multielement metallic systems: atomic size mismatch ( $\delta$ ), electronegativity difference ( $\Delta\chi$ ), valence electron concentration (VEC or  $e/a$ ), and enthalpy of mixing ( $\Delta H_{\text{mix}}$ ), etc.

Mizutani and his collaborators carried out an in-depth revision of the Hume-Rothery rules [6–8]. This work was based upon calculations of the electronic structure and densities of states, using a full-potential linearized augmented plane wave (FPLAPW) approximation. A very large series of binary compounds, with one having up to 1168 atoms per unit cell, was scrutinized. First, the authors found that contact between the Fermi sphere and specific facets of the Brillouin zone was responsible for the formation of a pseudogap whose depth and location in energy space in the vicinity of the Fermi energy were responsible for the stability of each specific compound. Second, hybridization between  $sp$  and  $d$  orbitals

adds to that selection, an effect that could be exemplified in many compounds containing transition metals. Finally, the respective contribution of the many elemental constituents to the valence band could be precisely evaluated, with results that depart significantly from data published earlier in relation to the discovery of stable Al-Cu-Fe quasicrystals [9]. Such systems are found in ternary, or multinary, alloys of generic composition  $A_xB_yC_z$  and are characterized by two important key facts: (i) the binary components A-B and A-C form well-defined compounds (negative formation enthalpy) and (ii) the B-C pair forms no compound nor solid solution, as B and C are immiscible due to the positive formation or mixing enthalpy. Such alloys are coined “push-pull” alloys [10]. A well-known example is the already mentioned, Al-Cu-Fe system [11], in which several binary Al-Cu and Al-Fe compounds are known, with some being rather complex. Based on the Cu-Fe phase diagram, these two constituents are known to be immiscible. A quasicrystal is found in the Al-rich corner of the phase diagram, in the vicinity of the simple  $\omega$ -Al<sub>7</sub>Cu<sub>2</sub>Fe crystal having 48 atoms in its unit cell. From a macroscopic standpoint, such ternary alloys act as complexity amplifiers, roughly analogic to push-pull amplifiers in electronics. The same situation is observed in other well-known quasicrystal forming alloys, such as Al-Cu-Li, Al-Mg-Zn, Al-Co-Cu, and a periodic complex metallic alloy Al-Cu-Ta with more than 27,000 atoms in a unit cell.

Here, we focused on the ternary Cu-Gd-Ca system, which shows great potential for the formation of complex compounds via the push-pull mechanism. Namely, there is more than a 99.6% miscibility gap for the elements Ca and Gd which means that they form neither a stable compound nor a solid solution. Even more so, up to date, no phase diagram is available for the Gd-Ca system. Immiscibility in the liquid phase has been observed by Kato and Copeland [12] and Gschneidner and Calderwood [13]. At the same time, Cu-Gd [14–16] and Cu-Ca [17, 18] form stable compounds, which was already reported back in the 1980s.

Up to date, we discovered no quasicrystal or complex structure in the Cu-Gd-Ca system. Instead, intermixing of Cu<sub>5</sub>Gd and Cu<sub>5</sub>Ca compounds in the solid state was observed, yet only through rapid quenching. Thus, in this paper, we report on the synthesis, structure, and stability of the Cu<sub>5</sub>Gd<sub>1-x</sub>Ca<sub>x</sub> ( $x = 0, 0.33, 0.5, 0.66, 1$ ) system. We also provide results about loading the samples with hydrogen, which changes the crystal structure.

## 2. Experimental

Our experimental study investigated five samples with the general formula Cu<sub>5</sub>Gd<sub>1-x</sub>Ca<sub>x</sub> ( $x = 0, 0.33, 0.5, 0.66, 1$ ), which were prepared by arc-melting and melt-spinning in high-purity (99.9999%) argon gas. First, copper and gadolinium pieces were arc-melted to form a eutectic alloy into which small pieces of pure Ca were added, carefully mastering the dissolution of this element into the liquid bath since calcium is extremely volatile. The arc-melted precursors were then spun on a rotating copper wheel at 40 m/s tangential speed using boron-nitride-coated graphite

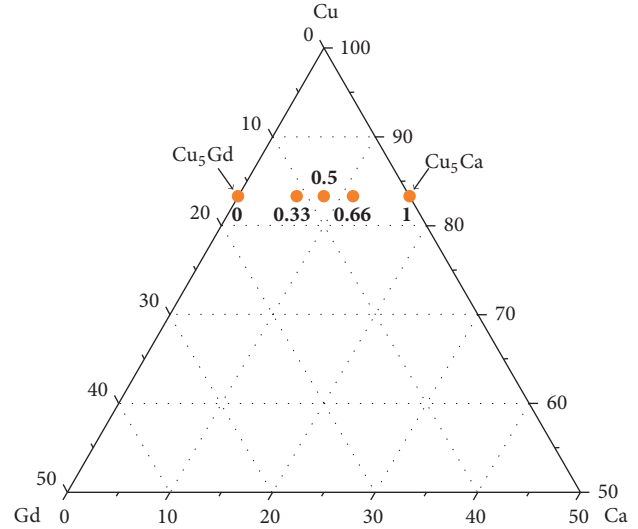


FIGURE 1: The Cu-rich half of the Cu-Gd-Ca ternary concentration chart with the studied Cu<sub>5</sub>Gd<sub>1-x</sub>Ca<sub>x</sub> compositions marked by dots, near to which  $x$  values are given.

crucibles to prevent the formation of any carbide phases in the ribbons. In order to minimize Ca evaporation, we increased the pressure in the melt-spinning chamber from the standard 700 mbar value to a pressure of 1500 mbar. In spite of this precaution, 2–3 wt.% of excess Ca had to be added to maintain the stoichiometry. The X-ray diffraction (XRD) patterns were recorded using a PANalytical diffractometer with Cu-K $\alpha$  radiation in the  $2\theta$  interval 2–60°. In situ XRD experiments were performed at set temperatures of 400, 580, and 700°C, using a heating rate of 20°C min<sup>-1</sup>. Anton Paar high temperature oven chamber 1200 N was used for high temperature measurements. Differential scanning calorimetry (DSC) was performed using a Netzsch STA 449 C/6/G Jupiter® apparatus and a sample mass of the order of few tens of milligrams. The temperature scheme was as follows: 20°C min<sup>-1</sup> up to 800°C, natural cooling down to 200°C, and then heating up again at 20°C min<sup>-1</sup> to 800°C in order to investigate the reversibility of the observed phenomena. TEM investigations were performed on a Jeol JEM ARM 200 CF microscope. The sample preparation included mechanical grinding and dimpling using isopropanol to avoid oxidation and subsequent Ar ion-milling. Hydrogenation was performed under 1 bar of 99.999% hydrogen gas at 300°C for 16 hours. Gas Analytical System QMS 403 C Aëolos (STA 449 C/6/G Jupiter, QMS 403 C, Netzsch, Germany) thermal analyzer with an attached mass spectrometer was used to perform mass-spectrometry of desorbed hydrogen from hydrogenated samples by 20°C min<sup>-1</sup> heating up to 800°C.

## 3. Results and Discussion

The compositions of the prepared samples are plotted on a partial Cu-Gd-Ca ternary concentration chart in Figure 1, that is, Cu<sub>5</sub>Gd<sub>1-x</sub>Ca<sub>x</sub> ( $x = 0, 0.33, 0.5, 0.66, 1$ ).

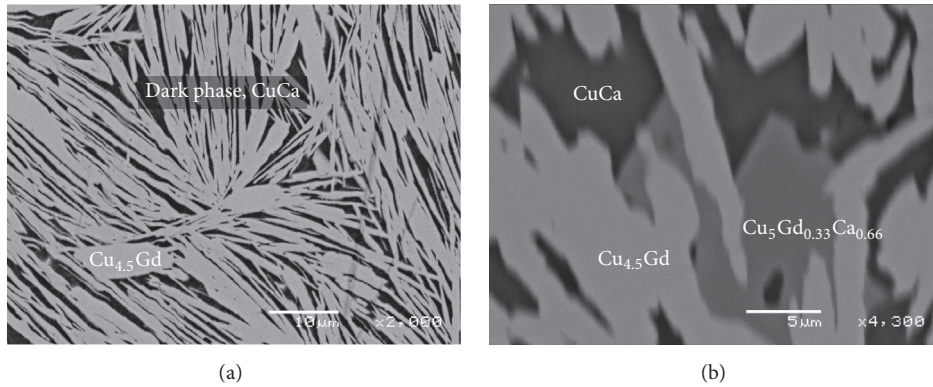


FIGURE 2: Backscattered SEM images of polished surface of (a) arc-melted  $\text{Cu}_5\text{Gd}_{0.5}\text{Ca}_{0.5}$  sample, and (b) the same sample after 7 days of homogenization at  $700^\circ\text{C}$  in an argon-filled sealed silica tube and subsequently ice-water quenched.

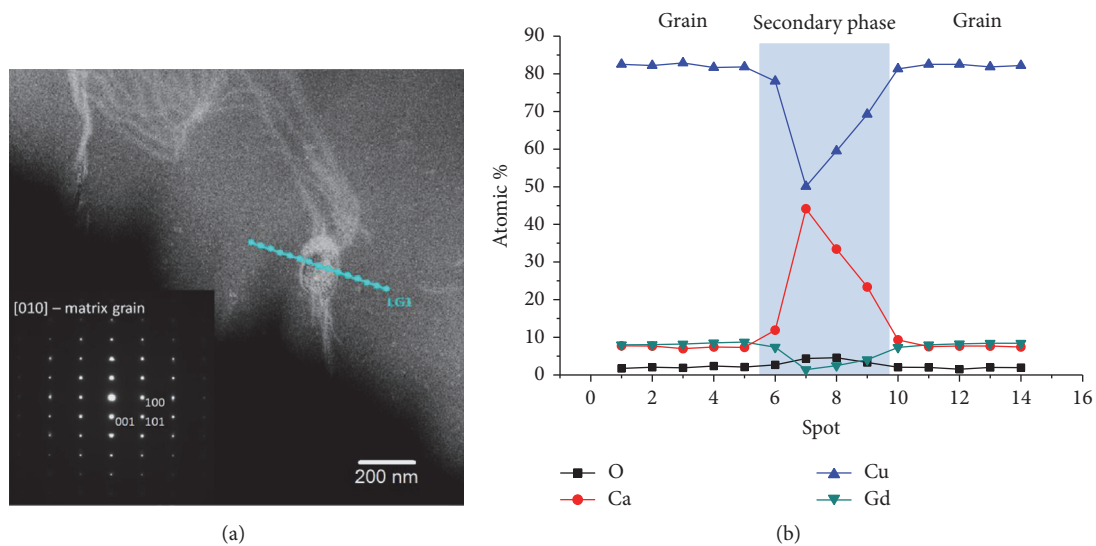


FIGURE 3: (a) Cross section image in STEM mode of a  $\text{Cu}_5\text{Gd}_{0.5}\text{Ca}_{0.5}$  melt-spun ribbon showing that the matrix grains have hexagonal symmetry (SAED). Also, a negligible amount of secondary Cu-Ca phase was found; (b) EDS line scan (14 points) confirmed stoichiometric, that is, nominal, composition of the matrix phase, low oxygen level, and segregation of Cu-Ca phase.

**3.1. Microstructure.** Figure 2(a) shows a microstructure of the arc-melted  $\text{Cu}_5\text{Gd}_{0.5}\text{Ca}_{0.5}$  sample. There is clear evidence in favor of a strong phase separation at slow cooling rate, since the two immiscible Gd and Ca constituents do not coexist in a single phase after a large amount of Cu has been added. The bright phase is  $\text{Cu}_{4.5}\text{Gd}$ , whereas the dark phase is the equiatomic Cu-Ca compound.

In an attempt to produce the very first ternary phase of this system, we homogenized the arc-melted button in a sealed silica tube containing a Ti-getter (which reacts with residual oxygen in the Ar gas) under highly pure argon gas at  $700^\circ\text{C}$  for 7 days, and subsequently ice-water quenched the ampoule. A backscattered SEM image with the associated EDS analyses is shown in Figure 2(b). Beside the bright  $\text{Cu}_{4.5}\text{Gd}$  phase, we observed  $\sim 1$  at.% of Gd dissolved in a dark Cu-Ca phase and, more importantly, a new ternary intermetallic compound with an intermediate Z-contrast with composition  $\text{Cu}_5\text{Gd}_{0.33}\text{Ca}_{0.66}$  was found. This result was used in another study to produce a single grain of that phase

and study its intricate magnetic structure [19]. Thus, in order to obtain a single-phase  $\text{Cu}_5\text{Gd}_{0.33}\text{Ca}_{0.66}$  sample, we used a rapid quenching technique, that is, melt-spinning, for its preparation. This method proved successful since backscattered SEM imaging and EDS analysis revealed a single-phase material with nominal stoichiometric composition. The same results were obtained for the other four samples dealt with in this article.

In order to check whether the melt-spun ribbons were completely homogeneous on the nanoscale, we performed a TEM characterization of the as-spun sample with  $x = 0.5$ . Our data are shown in Figure 3. Minor amount of Cu-Ca secondary phase was found to coexist in the matrix phase that had a stoichiometric  $\text{Cu}_5\text{Gd}_{0.5}\text{Ca}_{0.5}$  composition. Using SAED we confirmed the hexagonal structure of the matrix phase, which is in agreement with the XRD results. The population of the secondary phase was below the detection limit of XRD.

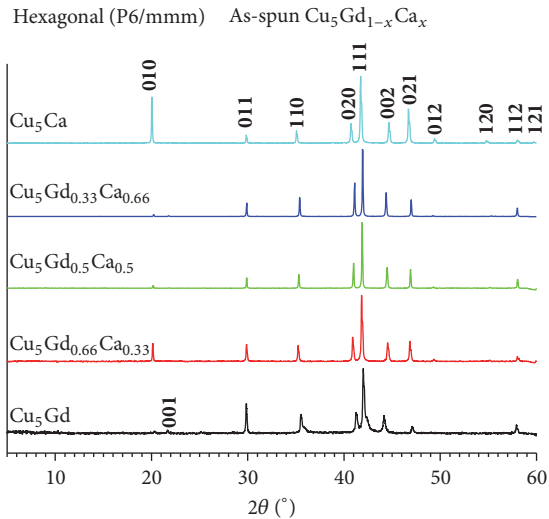


FIGURE 4: XRD patterns of  $\text{Cu}_5\text{Gd}_{1-x}\text{Ca}_x$  ( $x = 0, 0.33, 0.5, 0.66,$  and  $1$ ) ribbons, melt-spun at a tangential speed of the copper wheel of  $40 \text{ m/s}$ .

The amount of oxygen detected in the matrix phase was  $2 \text{ at.}\%$ , while in the Cu-Ca secondary phase it was  $5 \text{ at.}\%$ , which both can be attributed to surface oxidation during the TEM sample preparation.

**3.2. X-Ray Diffraction.** XRD patterns of the as-spun ribbons in Figure 4 indicate good mixing of the copper, gadolinium, and calcium constituents in the  $\text{Cu}_5\text{Gd}_{1-x}\text{Ca}_x$  system as pointed out by the preservation of the hexagonal structure as Gd is replaced by increasing amounts of Ca ( $x > 0$ ). For  $\text{Cu}_5\text{Gd}$ , two crystal modifications have been found in the phase diagram [14–16], namely, the high temperature (HT) hexagonal  $\beta\text{-Cu}_5\text{Gd}$  phase and the low temperature (LT) cubic  $\alpha\text{-Cu}_5\text{Gd}$  phase, whereas  $\text{Cu}_5\text{Ca}$  exists only in hexagonal polymorph [18]. Thus, it is clear that the large cooling rate associated with melt-spinning is crucial for the preparation of a single-phase material, that is, solid solutions of  $\text{Cu}_5\text{Gd}$  and  $\text{Cu}_5\text{Ca}$  compounds with hexagonal structure. Slight variations of peak positions in the XRD patterns, as well as differences in the relative intensities, were found along the sample series, particularly for the 010 peak. Peak shifts can be attributed to atom size effects which modify the lattice parameters, whereas the intensity changes reflect the respective influence of Ca replacing Gd onto the structure factor. Experimental data revealed that the unit cell volume of  $\text{Cu}_5\text{Ca}$  is  $1.65\%$  larger than that of  $\text{Cu}_5\text{Gd}$ . The apparently broader peaks in  $\text{Cu}_5\text{Gd}$  as opposed to other compositions may be related to smaller grain size and/or to disorder due to mechanical strains in the material.

When describing the dependence of lattice parameters and compositional factor  $x$ , we used Vegard's law [20], which holds that a linear relation exists, at constant temperature, between the crystal lattice parameters of a solid solution and the concentrations of the constituent elements (or binary compounds). Experimental dependence of hexagonal P6/mmm lattice parameters  $a$  and  $c$  on the compositional

factor  $x$  was found to be fairly linear. The lattice parameter  $a$  was decreasing with the addition of Ca while  $c$  was increasing (Figure 5(a)). This is a good example of Vegard's law, which demonstrates that replacement of Gd by Ca in the hexagonal compounds is random and substitutional. The unit cell volume increases linearly with  $x$  (Figure 5(b)). Figure 5(c) shows the P6/mmm unit cell of  $\text{Cu}_5\text{Gd}_{0.5}\text{Ca}_{0.5}$ , with equal occupancy of Gd and Ca atoms on the Ca1 sites in the  $\text{Cu}_5\text{Ca}$  prototype cell.

**3.3. Phase Stability, DSC, and HT XRD.** In order to assess the stability of these rapidly solidified alloys, we performed DSC and HT XRD measurements as previously described. Here, we show the results for  $x = 0, 0.5,$  and  $1$  samples only, as they are representative for the whole system. Figure 6 shows the DSC data and Figure 7 shows the HT XRD. All the recorded DSC peaks were due to irreversible transformations since none of them was observed again upon cooling and, later, upon a second heating run. A weak low- $T$  exothermic signal at  $367^\circ\text{C}$  ( $x = 0$ ) or  $350^\circ\text{C}$  ( $x = 1$ ) was found. Due to the exothermal nature of those peaks and the fact that the samples were rapidly solidified, they could be attributed to the relaxation of structural stresses.

Additionally, two endothermic DSC peaks were determined at  $560$  and  $657^\circ\text{C}$  for pure  $\text{Cu}_5\text{Ca}$ . According to the Cu-Ca phase diagram reported by Chakrabarti and Laughlin [18], we could attribute the  $560^\circ\text{C}$  peak to the peritectic reaction  $\text{Cu}_5\text{Ca} + \text{L} \leftrightarrow \beta\text{-Cu-Ca}$ , which occurs at  $567^\circ\text{C}$ . The peak at  $657^\circ\text{C}$  was most likely due to the melting of aluminum, which formed upon reduction of the alumina pot by segregated calcium metal. The exothermic Ca oxidation peak must therefore be hidden behind this peak, which results in a lower apparent melting enthalpy of aluminum.

In order to check if any structural changes occurred at elevated temperatures, we performed an in situ XRD analysis at the temperatures at which each DSC peak was ending, that is,  $400, 580,$  and  $700^\circ\text{C}$  (Figures 7(a)–7(c)).

The high temperature XRD data shown in Figure 7 point out that the two diffraction peaks of the Fm-3m cubic structure appear above  $400^\circ\text{C}$ . Its lattice parameter linearly increases with the temperature due to thermal expansion. Extrapolation to room temperature gave a value for the cubic lattice parameter  $a = 3.615 \text{ \AA}$ , which corresponds to the lattice parameter of pure copper. Since the relative intensity of Cu peaks increases with temperature, we concluded that we deal with diffusion-controlled copper segregation where the DSC signal of this process is smeared over a wide temperature range and thus cannot be observed. Also, in the case of the  $\text{Cu}_5\text{Ca}$  sample, the hexagonal phase peaks were still present at  $700^\circ\text{C}$ , suggesting that Cu segregation is inhibited due to higher stability of hexagonal  $\text{Cu}_5\text{Ca}$ . In the  $\text{Cu}_5\text{Gd}$  XRD, no LT phase peaks were observed upon heating. Note that the broad XRD peaks observed at low angles are not related to the sample but are caused by the kapton foil that the X-ray beam crosses on the way to the sample chamber.

Based on the combination of the DSC and the XRD data, we concluded that the ternary alloys are stable at least until  $400^\circ\text{C}$  since the XRD showed no phase separation to Cu-Gd and Cu-Ca binaries. However, at higher temperatures,

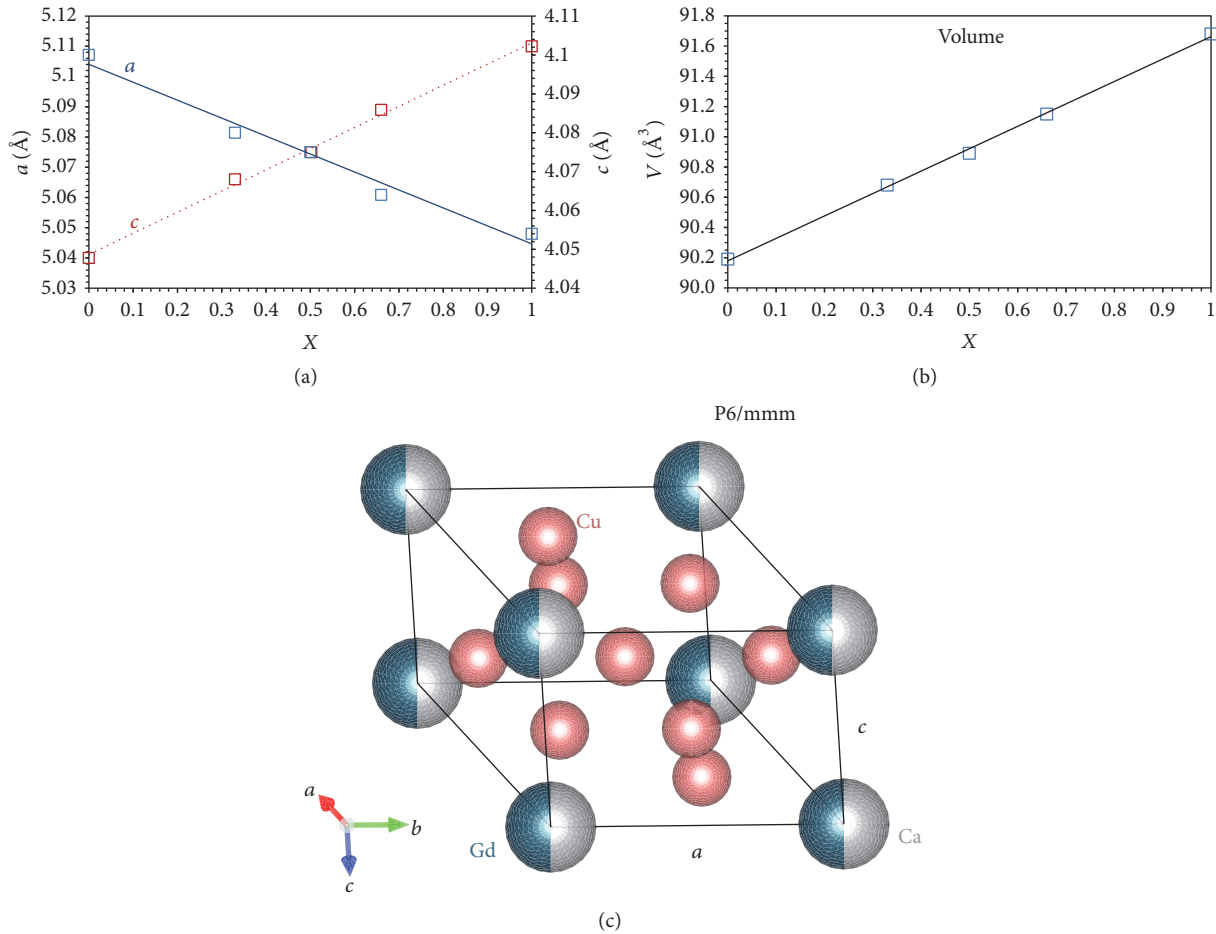


FIGURE 5: (a) P6/mmm lattice parameters  $a$  and  $c$  as functions of Ca concentration  $x$  in  $\text{Cu}_5\text{Gd}_{1-x}\text{Ca}_x$  compounds and (b) corresponding unit cell volume. The lines serve to guide the eyes. Error bars along  $x$ - and  $y$ -axes are within the size of the data points; (c) P6/mmm unit cell of  $\text{Cu}_5\text{Gd}_{0.5}\text{Ca}_{0.5}$ .

severe copper segregation to the surface of the ribbons occurred, particularly in the  $x = 0$  sample, and consequently oxidation of residual Gd as decomposition product, upon which cubic  $\text{Gd}_2\text{O}_3$  (1a-3,  $a = 1.0790$  nm) has formed. Additional indication for Gd-oxide formation is that the corresponding diffraction peaks positions are independent of the temperature, which is related to low thermal expansion coefficient of ceramic materials. On the contrary, peaks of metallic Cu shift to higher  $d$ -values with temperature. The existence of other secondary phases like  $\text{Cu}_6\text{Gd}$  (orthorhombic, Pnma,  $a = 0.8315$  nm,  $b = 0.5983$  nm,  $c = 0.9949$  nm) and (nanostructured) Cu-oxides cannot be excluded, but the exact phase identification is complicated due to poor definition of the background axis very common in this type of experiments in which the primary, rather than the diffracted, beam has been collimated by a crystal monochromator [21].

In the case of the  $x = 1$  sample, no peritectically formed  $\beta$ -Cu-Ca phase could be found because it melts at  $580^\circ\text{C}$  (and forms peritectically at  $567^\circ\text{C}$ ). Instead, XRD peaks of CaO were found. This phase is cubic Fm-3m,  $a = 0.481$  nm, and most likely formed from segregated Ca from the liquid phase and oxygen as impurity in the Ar carrier gas flowing in the HT XRD chamber. Since the  $x = 0.5$  sample contains a lower

amount of  $\text{Gd}_2\text{O}_3$  and no CaO, it can be concluded that (i) the addition of Ca to  $\text{Cu}_5\text{Gd}$  stabilizes the hexagonal phase and (ii) the addition of Gd to the  $\text{Cu}_5\text{Ca}$  system prevents liquid phase formation during heating up to  $700^\circ\text{C}$  and thus Ca oxidation. This way, ternary alloys turn out to be more stable than both binaries.

**3.4. Hydrogenation.** After exposing the as-spun hexagonal samples to pure hydrogen atmosphere at  $300^\circ\text{C}$  for 16 hours, approximately 0.5 wt.% of desorbed hydrogen was released from all samples upon subsequent dehydrogenation. XRD analysis of  $\text{Cu}_5\text{Gd}_{1-x}\text{Ca}_x$  hydrides (Figure 8(a)) revealed a multiphase formation rather than hexagonal crystal lattice expansion upon hydrogenation. In case of binary alloys, we determined pure Cu and  $\text{GdH}_2$  ( $x = 0$ ) or  $\text{CaH}_2$  ( $x = 1$ ) peaks. Formation of Gd hydride ( $\text{Gd} + \text{H}_2 \rightarrow \text{GdH}_2$ ) has already been observed by Hruška et al. [22], whereas Ca reaction with hydrogen ( $\text{Ca} + \text{H}_2 \rightarrow \text{CaH}_2$ ) was investigated by Sturdy and Mulford [23], and Rittmeyer and Wietelmann [24]. Copper hydride has been previously found to form from elemental copper only under severe pressure around 20 GPa [25], so it is reasonable to assume that protons do not react with copper atoms in our alloys at given hydrogenation

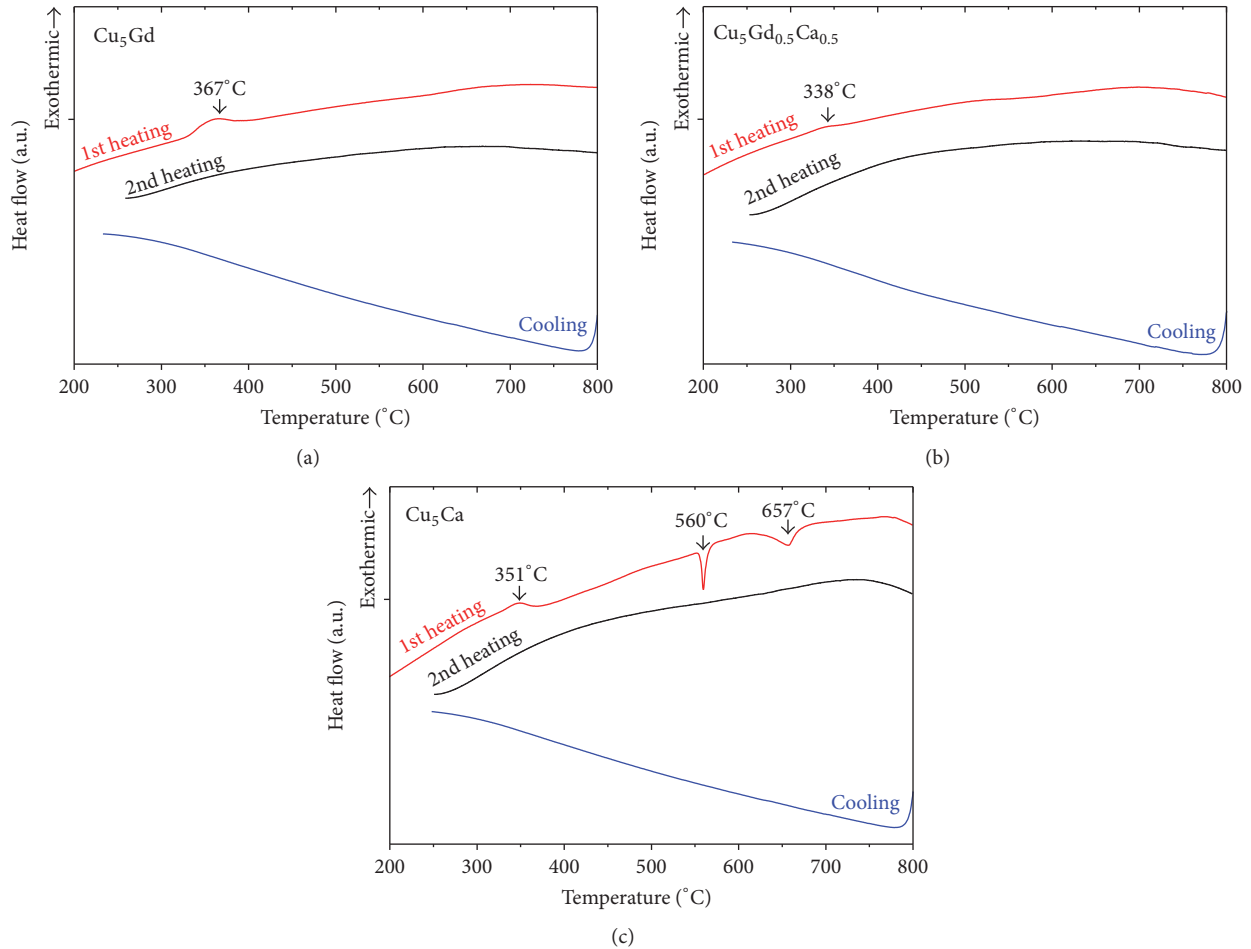


FIGURE 6: DSC analysis of  $\text{Cu}_5\text{Gd}_{1-x}\text{Ca}_x$  ( $x = 0, 0.5,$  and  $1$ ) melt-spun ribbons during two-stage heating experiments.

conditions. In fact, this might be the driving force behind the severe phase separation we observed.

In all three ternary systems, we noticed the appearance of a novel phase which appears to be a  $\text{H}_2\text{Gd}_{1-x}\text{Ca}_x$ -based solid solution, coexisting with pure Fm-3m Cu. As seen in Figure 8(a), all XRD peaks of  $\text{GdH}_2$  were shifting to lower angles as the amount of Ca was increasing. Thus, a cubic solid solution of  $\text{GdH}_2$  and  $\text{CaH}_2$  compounds must have formed; otherwise, their separated peaks would appear with peak intensity depending on  $x$ . In addition, Figure 8(b) shows that the  $\text{H}_2$  mass-spectra of  $x = 0.33, 0.5,$  and  $0.66$  samples are not linear combinations of those of  $\text{GdH}_2$  and  $\text{CaH}_2$  (which would be the case if the system consisted of grains of individual hydrides). In order to check if the hydride solid solution contains any Cu, high-resolution EDS mapping or STEM analysis should be performed. However, in case of hydrogenated  $\text{Cu}_5\text{Gd}$ , we found pure Cu and  $\text{GdH}_2$ . If the latter contained some copper, it would definitely be seen as a shift of XRD peaks. The same conclusion holds for  $\text{Cu}_5\text{Ca}$  and corresponding  $\text{CaH}_2$ .

Nuclear magnetic resonance (NMR) is a technique per excellence to study proton mobility in a material. Therefore, to investigate how the Ca concentration in the  $\text{Cu}_5\text{Gd}_{1-x}\text{Ca}_x$

system (or rather  $\text{H}_2\text{Gd}_{1-x}\text{Ca}_x$ ) affects the interaction of protons with the host metallic lattice and interpret Figure 8(b) through proton diffusivity and hopping activation energies, we measured the proton spin-lattice relaxation by means of  $^1\text{H}$  NMR at proton resonance frequency of 500 MHz, corresponding to a magnetic field of 11.75 Tesla. We used a superconducting Bruker magnet and an  $^1\text{H}$  probe, with samples being placed in 5 mm glass tubes. Proton hopping between the interstitial sites causes fluctuations in the interproton spin interactions and activation energy for these jumps can be obtained from the temperature dependence of the proton spin-lattice relaxation time  $T_1$  [26]. However, it turns out that proton relaxation time  $T_1$  is roughly temperature-independent in the temperature range from room temperature to  $120^\circ\text{C}$  (the highest temperature achievable in the setup). In this temperature range, rapid proton hopping is expected. However, the temperature-independent spin-lattice relaxation indicates that the dynamic contribution to proton relaxation is masked by another contribution, perhaps due to proton coupling to paramagnetic centers in the sample, such as defects in the crystal structure or individual Gd atoms with their paramagnetic moment unshaded by the free

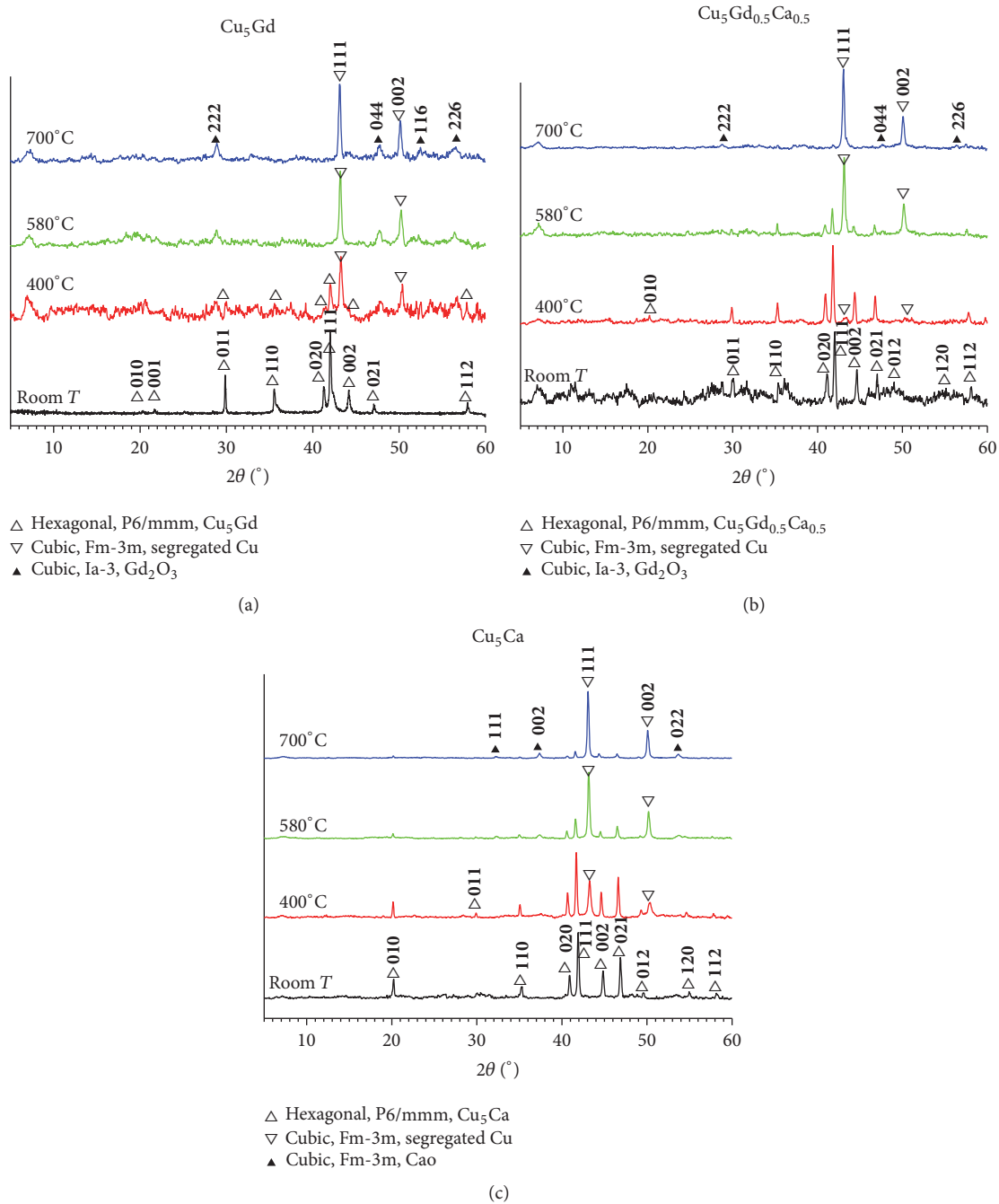


FIGURE 7: (a–c) High temperature XRD patterns of  $\text{Cu}_5\text{Gd}_{1-x}\text{Ca}_x$  melt-spun ribbons recorded at room temperature, 400, 580, and 700°C; (a)  $x = 0$ , (b)  $x = 0.5$ , and (c)  $x = 1$ .

electron gas. Therefore, no information about the activation energies for jumps could be obtained by  $^1\text{H}$  NMR.

#### 4. Conclusion

We prepared a series of melt-spun ribbons by substitution of Gd with Ca in a  $\text{Cu}_5\text{Gd}$  master alloy. After rapid quenching by melt-spinning, all samples exhibited hexagonal P6/mmm structure regardless of the Gd/Ca ratio, which implies good

substitutional solid solubility of Ca and Gd in the system with 83.3 at.% of Cu. This result is in accordance with results published by Carnasciali et al. [15] and Subramanian and Laughlin [16] who reported that the high temperature polymorph of the  $\text{Cu}_5\text{Gd}$  compound has hexagonal P6/mmm  $\text{Cu}_5\text{Ca}$ -like structure ( $a = 0.504$  nm,  $c = 0.411$  nm). No ternary Cu-Gd-Ca compound synthesis was reported so far, except the  $\text{Cu}_5\text{Gd}_{0.54}\text{Ca}_{0.42}$  single crystal, which was grown by parallel collaborating group [19] upon findings reported here and published prior to the present publication.

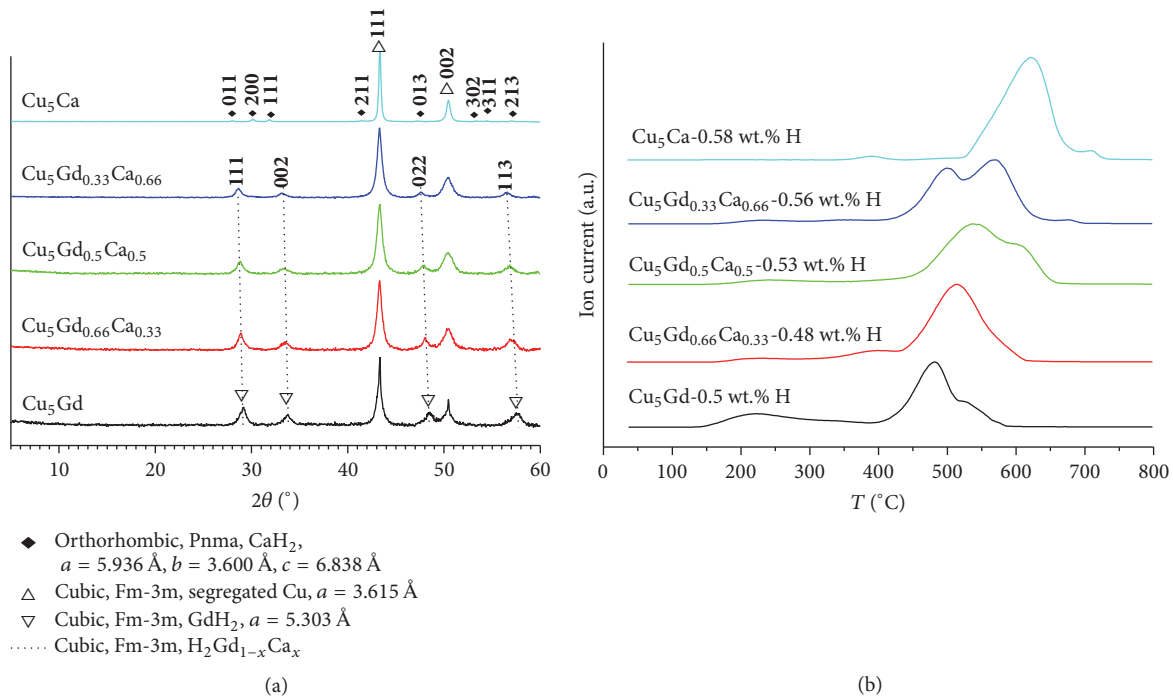


FIGURE 8: (a) XRD patterns of hydrogenated  $\text{Cu}_5\text{Gd}_{1-x}\text{Ca}_x$  ( $x = 0, 0.33, 0.5, 0.66,$  and  $1$ ) melt-spun ribbons and (b) corresponding mass-spectra of thermally desorbed hydrogen gas.

Transmission electron microscopy of the melt-spun ribbon with  $x = 0.5$  revealed homogeneity on the nanoscale of  $\text{Cu}_5\text{Gd}_{0.5}\text{Ca}_{0.5}$  matrix phase, although minor amounts of Cu-Ca precipitates were discovered, which did not influence significantly the stoichiometry of the matrix phase. Copper segregation was observed in all investigated samples upon heating by in situ XRD. Regardless of Cu segregation, the ternary alloys seem more stable or corrosion resistant, as the amounts of  $\text{Gd}_2\text{O}_3$  and CaO secondary phases were suppressed. The later was found only in  $x = 1$  sample.

Copper segregation was also observed upon loading the samples with hydrogen. Cubic  $\text{Fm-3m}$   $\text{H}_2\text{Gd}_{1-x}\text{Ca}_x$ -based solid solution was identified from the XRD measurements and the mass-spectra of thermally desorbed hydrogen gas. EDS measurements uncovered the presence of oxide species; however, their size was beneath the resolution of XRD. A proton mobility study in the hydride phase was attempted by means of NMR but the activation energy for proton hopping was not possible to obtain since the proton spin-lattice relaxation is completely dominated by paramagnetic centers in the system.

## Conflicts of Interest

The authors declare no conflicts of interest.

## Acknowledgments

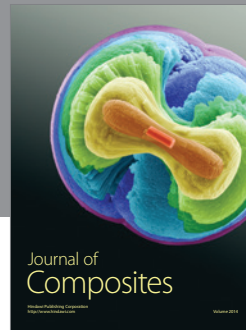
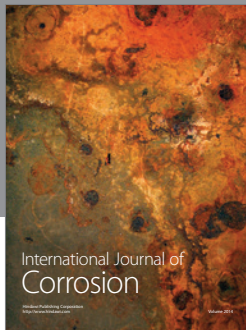
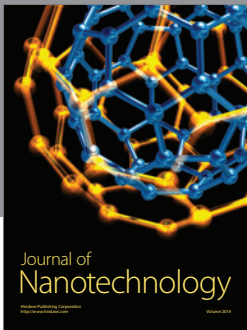
This research was part of the bilateral French-Slovenian PROTEUS project CalGad-X. The authors are grateful to Dr. Marjeta Maček for assistance in DSC and mass-spectrometry

experiments and to Ms. Urška Kavčič for performing catalytic tests under controlled atmosphere. The authors acknowledge the financial support from the Slovenian Research Agency (research core funding no. P2-0152) and CNRS PICS “CalGad-X”.

## References

- [1] B. S. Murty, J.-W. Yeh, and S. Ranganathan, *High-Entropy Alloys*, Butterworth-Heinemann (Elsevier), London, UK, 1st edition, 2014.
- [2] A. Takeuchi and A. Inoue, “Quantitative evaluation of critical cooling rate for metallic glasses,” *Materials Science and Engineering: A*, vol. 304-306, pp. 446–451, 2001.
- [3] Y. Zhang, Y. J. Zhou, J. P. Lin, G. L. Chen, and P. K. Liaw, “Solid-solution phase formation rules for multi-component alloys,” *Advanced Engineering Materials*, vol. 10, no. 6, pp. 534–538, 2008.
- [4] S. Guo, C. Ng, J. Lu, and C. T. Liu, “Effect of valence electron concentration on stability of fcc or bcc phase in high entropy alloys,” *Journal of Applied Physics*, vol. 109, no. 10, Article ID 103505, 2011.
- [5] S. Guo, Q. Hu, C. Ng, and C. T. Liu, “More than entropy in high-entropy alloys: forming solid solutions or amorphous phase,” *Intermetallics*, vol. 41, pp. 96–103, 2013.
- [6] U. Mizutani, M. Inukai, H. Sato, and E. S. Zijlstra, “Hume-Rothery stabilization mechanism and e/a determination for RT- and MI-type 1/1-1/1-1/1 approximants studied by FLAPW-Fourier analyses,” *Chemical Society Reviews*, vol. 41, no. 20, pp. 6799–6820, 2012.

- [7] U. Mizutani, M. Inukai, H. Sato, and E. S. Zijlstra, "Hume-Rothery stabilization mechanism and  $\epsilon/a$  determination in MI-type Al–Mn, Al–Re, Al–Re–Si, Al–Cu–Fe–Si and Al–Cu–Ru–Si 1/1-1/1-1/1 approximants—a proposal for a new Hume-Rothery electron concentration rule," *Philosophical Magazine*, vol. 92, no. 13, pp. 1691–1715, 2012.
- [8] U. Mizutani, *Hume-Rothery Rules for Structurally Complex Alloy Phases*, CRC Press, Boca Raton, Fla, USA, 2010.
- [9] A.-P. Tsai, "Discovery of stable icosahedral quasicrystals: progress in understanding structure and properties," *Chemical Society Reviews*, vol. 42, no. 12, pp. 5352–5365, 2013.
- [10] J.-M. Dubois, E. Belin-Ferré, and A. P. Tsai, "Quasicrystals and complex metallic alloys," in *Kirk-Othmer Encyclopedia of Chemical Technology*, pp. 1–19, John Wiley & Sons, 2016.
- [11] F. Faudot, A. Quivy, Y. Calvayrac, D. Gratias, and M. Harmelin, "About the Al–Cu–Fe icosahedral phase formation," *Materials Science and Engineering: A*, vol. 133, pp. 383–387, 1991.
- [12] H. Kato and M. I. Copeland, "USBM-U-952," Metallurgical Progress Report 15, National Technical Information Service, Springfield, Va, USA, 1962.
- [13] K. A. Gschneidner and F. W. Calderwood, "The Ca–Gd (Calcium–Gadolinium) system," *Bulletin of Alloy Phase Diagrams*, vol. 8, no. 6, article 515, 1987.
- [14] H. Okamoto, *Desk Handbook: Phase Diagrams for Binary Alloys*, ASM International, Geauga County, Ohio, USA, 2nd edition, 2010.
- [15] M. M. Carnasciali, S. Cirafici, and E. Franceschi, "On the Gd–Cu system," *Journal of The Less-Common Metals*, vol. 92, no. 1, pp. 143–147, 1983.
- [16] P. R. Subramanian and D. E. Laughlin, "The Cu–Hf (copper–hafnium) system," *Bulletin of Alloy Phase Diagrams*, vol. 9, no. 1, pp. 51–56, 1988.
- [17] F. Merlo and M. L. Fornasini, "The structures of  $\alpha$ -CaCu,  $\beta$ -CaCu, SrAg and BaAg: four different stacking variants based on noble-metal-centred trigonal prisms," *Acta Crystallographica B*, vol. 37, no. 3, pp. 500–503, 1981.
- [18] D. J. Chakrabarti and D. E. Laughlin, "The Ca–Cu (Calcium–Copper) system," *Bulletin of Alloy Phase Diagrams*, vol. 5, no. 6, pp. 570–576, 1984.
- [19] M. Krnel, S. Vrtnik, P. Koželj et al., "Random-anisotropy ferromagnetic state in the  $\text{Cu}_5\text{Gd}_{0.54}\text{Ca}_{0.42}$  intermetallic compound," *Physical Review B*, vol. 93, no. 9, Article ID 094202, 2016.
- [20] A. R. Denton and N. W. Ashcroft, "Vegard's law," *Physical Review A*, vol. 43, no. 6, pp. 3161–3164, 1991.
- [21] V. K. Pecharsky and P. Y. Zavalij, *Fundamentals of Powder Diffraction and Structural Characterization of Materials*, Springer, Berlin, Germany, 2nd edition, 2009.
- [22] P. Hruška, J. Čížek, P. Dobroň et al., "Investigation of nanocrystalline Gd films loaded with hydrogen," *Journal of Alloys and Compounds*, vol. 645, no. 1, pp. S308–S311, 2015.
- [23] G. E. Sturdy and R. N. R. Mulford, "The gadolinium–hydrogen system," *Journal of the American Chemical Society*, vol. 78, no. 6, pp. 1083–1087, 1956.
- [24] P. Rittmeyer and U. Wietelmann, "Hydrides," in *Ullmann's Encyclopedia of Industrial Chemistry*, Wiley-VCH, Weinheim, Germany, 2002.
- [25] C. Donnerer, T. Scheler, and E. Gregoryanz, "High-pressure synthesis of noble metal hydrides," *Journal of Chemical Physics*, vol. 138, no. 13, Article ID 134507, 2013.
- [26] A. Gradišek and T. Apih, "Hydrogen dynamics in partially quasicrystalline  $\text{Zr}_{69.5}\text{Cu}_{12}\text{Ni}_{11}\text{Al}_{7.5}$ : a fast field-cycling relaxometric study," *Journal of Physical Chemistry C*, vol. 119, no. 19, pp. 10677–10681, 2015.



**Hindawi**

Submit your manuscripts at  
<https://www.hindawi.com>

